THE COUPLING OF WINDING MODELS AND ROLL QUALITY INSTRUMENTS

By

C. Mollamahmutoglu[1], O. Bulut[2], S. Adari[3] and J. K. Good[3]
[1]Yildiz Technical University, TURKEY
[2] International Technological University, TURKEY
[3]Oklahoma State University, USA

ABSTRACT

Winding models have been under development for roughly 50 years. These models have become mature in their ability to predict the internal residual stresses within a wound roll as a function of winder type, winder operating parameters, web and core material parameters and non-uniformity inherent in the web. The internal stresses are useful when predicting winding defects. The majority of the instruments that have been developed to infer the quality of rolls wound in production environments are dynamic hardness testers that provide output in unique units. These devices are very useful in the production environment for studying cross machine direction (CMD) variation of hardness in wound rolls. This variation could have resulted independently from web tension, nip load, web thickness, modulus or length non-uniformity in the CMD. It could also have resulted from combined non-uniformity from all of these sources but hardness testers have no means to determine the source of hardness variation. The coupling of winding models and dynamic roll hardness testers will move roll quality improvement to an advanced diagnostic level. We will demonstrate that it has become possible for winding models which have been extended with dynamic impact models to provide estimates of hardness in the unique units of any test instrument. Our goal is to promote improvement in roll quality by the combined use of winding models and dynamic hardness testers to minimize wound roll defects.

INTRODUCTION

Hand held instruments for the assessment of roll quality have common application place in web handling industry. In-site and quick assessment of various aspects of quality make them valuable tools. Among them, hardness related testers are most widely used ones. In fact hardness measurements started early in web handling production by using

sticks or clubs made from hardwood [1]. Hitting a completed roll at various CMD locations with a club or stick gave an idea of hardness to the shop floor personnel. The level of hardness were due to pitch of sound accompanying the impact or the vibrations sensed at the handle of the stick or sometimes combination of both. These early attempts clearly lacked in producing quantitative, objective and standardized results. Later, devices with carefully calibrated mechanisms and integrated electronic measurement equipment solved this problem. The results produced with these standardized tools are often represented in terms of device specific parameters for each tool. The working principles of hardness testers share common points. An impactor which is activated with a calibrated mechanism or just by an experienced operator hits outer surface of the roll and attached electronic measurement equipment records various velocities or accelerations during the impact event. These electronic signals are then used to produce device specific parameters which are related to fundamental engineering units or completely unique values. Finally device displays an objective value for the hardness at the impact location. Among these devices Beloit Rho-meter which was invented by D. Pfeiffer has been one of the most widely used [2]. The basic measurement unit for this device is the maximum attained deceleration during the impact as its impactor hits the surface of the roll. Rho-meter then converts deceleration to so called "Rho" units by setting 1 Rho = 3.76 g's where g is Earth's acceleration (≈ 9.81 m/s^2). The main disadvantage of Rho-meter is that it cannot be used for very soft (tissues, non-wovens) or very hard (metals) materials. Later a computerized, lighter and compact version of the Rho-meter which resembles a hammer called Rho-hammer is developed [3]. Working on the same max deceleration measurement this device lacks the repeatability since readings depend on how hard the operator strikes the roll. Thus considerable experience is required on operator side for correct assessment of quality. Another hammer like device used for quality assessment is Schmidt Hammer which retains on coefficient of restitution concept for addressing the hardness [1]. Initially developed for measuring the hardness of cured concrete Schmidt Hammer uses a calibrated spring loaded tip for impact. The rise of the tip after the impact (rebound) is recorded and converted to device specific "R" values on the display screen attached to the device. Another hardness device called Backtender's Friend is used for semi-automatic hardness testing along CMD of a roll. Being bulky and hard to use this device produces hardness values unique to the device rather than related to a fundamental engineering quantity like acceleration or velocity [1]. Above mentioned testers can damage sensitive and delicate web materials as local impact stresses can reach excessive values. Paro-tester which is also based on the concept of coefficient of restitution like Schmidt Hammer has an edge over others on this issue since it produces the smallest impact energy when compared with previous devices. Paro-tester measures the impact and rebound velocities and immediately calculates device specific "L" units which is related to the ratio of these velocities [1]. One way or the other calculated hardness values are not directly linked to the assessment of quality. In other words required hardness for preventing slippage or buckling inside a roll cannot be simply inferred from the recorded hardness values. Even considerable amount of experience with the device and product may not be enough to address quality standards for defect free product by only relying on hardness values. In fact analysis and preventing of defects and thus assessment of quality is based on direct engineering units of stresses and strains developing inside a roll. Wound-roll models have been developed to address these stress and strain fields under various conditions. Results obtained from these models can be directly related to the mechanical state of a wound roll and quality issues can be addressed directly [1]. But running on computers, simulations based on these models are not as practical as a hand-held device on the shop floor. Thus it appears to be

a gap between device produced hardness values and the engineering stresses and strains which directly relates to defects. The main aim of this study is to construct a bridge between these two approaches. Throughout this study we will also address the real physics behind hardness testing. Being a local measurement (hardness value is measured at the outer surface where the impact takes place) we will see whether it is consistent to use recorded hardness values as valid and effective numbers for an entire roll. In order to achieve these we modeled the hardness as a mechanical problem and produced various models in order to capture the physics of the impact event. Lab tests were also conducted on two different materials under various winding conditions in conjunction with modeling efforts. In our study selected device is Rho-meter. The plan of study follows: In the first chapter we will show our modeling efforts first by using a commercial finite element package called ABAQUS. Internal workings of Rho-meter is carefully ported to this modeling space by using 3D geometry of striker. Assuming well-known material nonlinearity of the wound roll in radial direction ABAQUS produced dynamic impact results which shows deceleration curves for the striker. Later we proposed a simple finite difference method for solving the 1D equation of motion which is written for roll and the striker by representing them as rigid bodies connected with springs. The nonlinearity of the roll spring is obtained from another study of the lead and the senior author [9]. We see that almost identical dynamic results were obtained compared with the sophisticated and demanding ABAQUS. An even simpler model based conservation of the mechanical energy is also developed which can be used to directly calculate the Rho values once the nonlinear spring parameters from [9] are used. In the second chapter testing efforts and results are demonstrated collectively from various models. Finally we showed simple models developed in this study can be incorporated into a winding model which then can be used to directly relate the stresses with Rho values. For this purpose a web material with measured persistent non-uniform CMD thickness profile is used and the integrated model results for hardness from an axisymmetric wound-roll model [6] are shown together with the test results obtained in lab. Thus we will show how to coupling developed between the hardness model and the winding model can be effectively used to address quality issues by demonstrating the CMD thickness non-uniformity case.

MODELING THE HARDNESS TESTING

Striker Side

In this study we have selected Beloit Rho-meter for the analysis of hardness problem. The modeling effort has two sides. One is the striker side the other is the wound roll side. Impact is a complex interaction between roll and the striker. Thus it is wiser to analyze the mechanics of the striker side first independently and make sure that we have a correct striker model which can be used on the roll side. In Figure 1 on the left we see the Rho-meter on a roll and on the right internal mechanism is shown when the casing is removed.

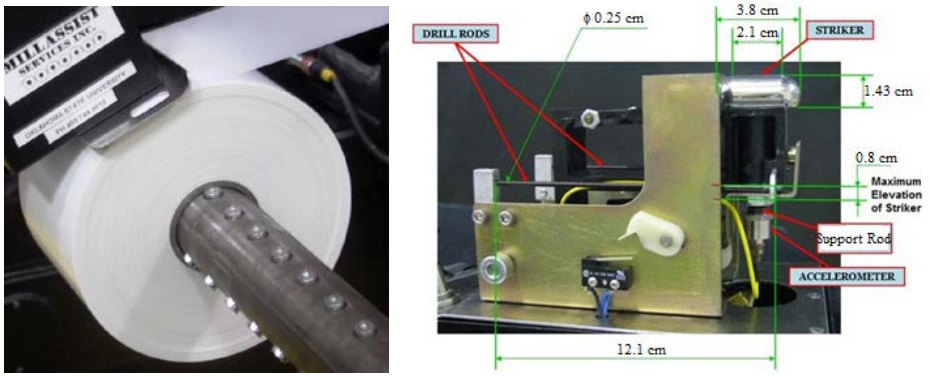

Figure 1 – Beloit Rho-meter on a Roll and Internal Mechanism

As it is observed that a cantilever spring mechanism is attached to a trigger which pulls the striker head to a certain height with respect to equilibrium position of the head. This is measured to be 0.8 cm. After releasing the striker it travels 0.24 cm further from the equilibrium position because of the metal plate attached to the bottom of the casing. During the impact an accelerometer attached to the striker head collects data. We have modeled the striker as a rigid shell which is given an effective mass and attached to spring which is given a stiffness equivalent to the stiffness of cantilever mechanism. Spring constant for the cantilever mechanism was easily obtained by a hand-held force gage. This effective spring stiffness is found to be $K_{eff} = 28\ N/cm$. Effective mass of the system is then obtained via natural frequency measurements. An oscilloscope which is attached to accelerometer output provides the frequency response when free vibration is induced. Natural frequency of the system was found to be $\omega_n = 149.5\ rad/s$ by measuring the duration between two consecutive peak accelerations observed on oscilloscope. Now effective mass can be easily obtained as $M_{eff} = 0.125\ kg$. using {1}:

$$M_{eff} = \frac{K_{eff}}{\omega_n^2} \qquad \{1\}$$

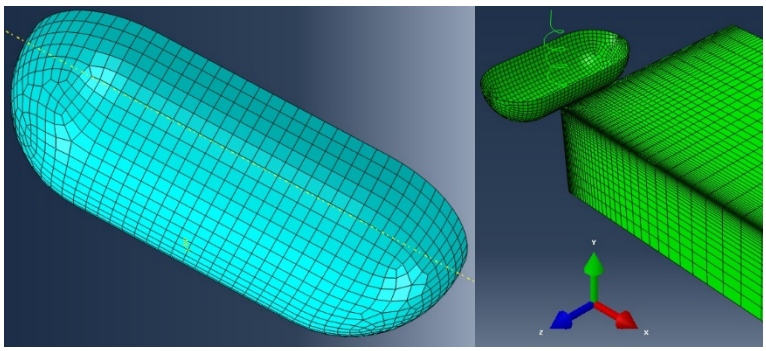

Figure 2 – Striker Head and ABAQUS Model

Figure 2 shows the striker head and ABAQUS model. We conducted static and dynamic tests in order to validate the spring mass representation for the Rho-meter. Static tests were completed via pressing the strikers head into dedicated rubber block which

comes with the device for calibration purposes. Hardness of the calibration block was measured with Durometer and (using international rubber hardness degrees) found to be 102 units (IRHD). This value is then converted to an elastic modulus value for the rubber via expression $E_{rubber} = 1446e^{0.0564*IRHD}$ (KPa) [7]. Load deformation values obtained from experiment are compared with the static simulation results coming from ABAQUS using rigid shell in Figure 3. Table 1 shows all the material and geometrical data.

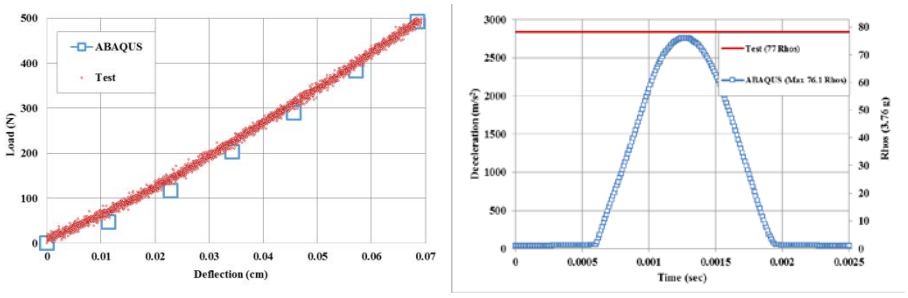

Figure 3 – Static and Dynamic Model and Test Comparisons for Striker

Rubber Block		STRIKER	
Hardness (IRHD)	102	Spring Stiffness (N/cm)	28
Young's Mod. (KPa)	44614	Mass (gr)	125
Poisson's Ratio	0.458	Release Position (cm)	0.8
Mass Density (gr/cm^3)	1.4	Impact Poistion (cm)	-0.24

Table 1 – Geometrical and Material Data for Calibration Block and Striker

As observed from Figure 3 superb agreement of the static test and model results indicates correct geometry is used. Figure 3 also shows dynamic testing and model results as well. Deceleration values calculated by ABAQUS were plotted with respect to time. ABAQUS max deceleration corresponded to 76.1 Rhos and due to device manual testing the device on calibration block should produce 77 Rhos. These two values are very close to each other thus we can also conclude that mass spring representation of the striker is correct.

Roll Side

Pressure dependent radial material property of the web materials is well known. That is radial modulus E_r is function of radial pressure σ_r. One of the most common representation is due to Pfeiffer [8]:

$$E_r = K_2(-\sigma_r + K_1) \qquad \{2\}$$

K_1 and K_2 are material constants with K_2 controlling the overall compressibility (softness) of the material. In this study two PET materials are used; one with high K_2 (low compressibility) and the other with low K_2 (high compressibility). These materials were wound into rolls with different web line tensions T_w. Table 2 includes all the material and geometrical data of the produced wound rolls. In Table 2 $G_{zr}=G_{tr}=2E_r$ assumption is

proven in and directly comes from one of our previous studies [9] which is concerned with nip contact analysis of wound rolls.

WEB	K_1(KPa)	K_2	E_z,E_t (MPa)	ρ (gr/cm^3)	R_{in} (cm)	R_{out} (cm)	Winding Tensions (N)
PET1	4.62	123.88	5681	1.4	4.45	13.34	26.7, 33.4, 40, 46.7
PET2	20.27	26.24	4950	1.4	4.45	13.34	26.7, 53.4, 80

WEB	G_{zr},G_{tr} (MPa)	G_{tz} (MPa)	ν_{tz}	ν_{tr},ν_{zr}	thickness (cm)	width (cm)	Steel Core Thickness (cm)
PET1	$2E_r$	2185	0.3	0	0.01	15.24	0.64
PET2	$2E_r$	1904	0.3	0	0.01	15.24	0.64

Table 2 – Material and Geometrical Data for PET Rolls used in The Study

3D ABAQUS Modeling

We have developed a 3D model of the wound roll. Fig 4. Shows the geometrical model in ABAQUS. Because of symmetry conditions (*y-z* plane $u_x=0$, *x-y* plane $u_z=0$) and locality (*x-z* plane $u_y=0$) of impact event only 1/8 of the roll is modeled. Core conditions are imposed as rigid that is for $x^2+y^2=(r_{core})^2$ and $0<z<width/2$ $u_x=u_y=u_z=0$.

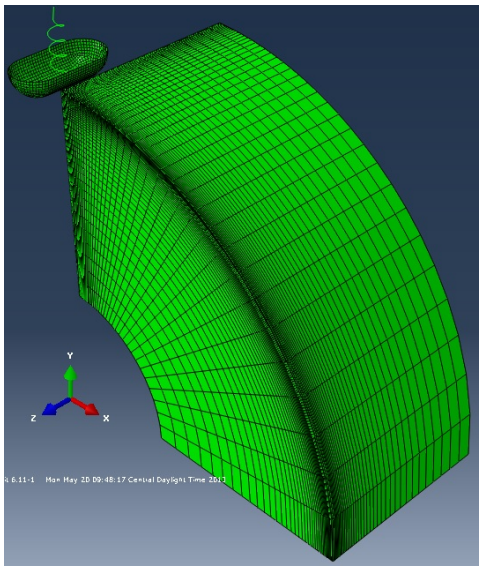

Figure 4 – 3D ABAQUS Model for Hardness Testing

As seen from Figure 4, in order to increase resolution at the impact location we have refined mesh. In ABAQUS edges seeds (dictating nodal refinement along an edge) are given with a bias when refinement is considered. Let *b* be the ABAQUS definition of bias ratio, *n* number of elements and *k* the ratio of length of neighbor segments on an edge then ABAQUS defines element lengths from coarse to fine as $h, kh, k^2h \ldots, k^{n-1}h$ with input bias ratio *b* as $b=1/k^{n-1}$. In this study there are 40x40x40 elements in R,θ,Z directions with different bias ratios for R (40,80,160,320), for θ (40), for Z (40). Pfeiffer's material model is not present in ABAQUS material library. Thus we developed a user defined material file (VUMAT) defining the relation between the radial modulus E_r and the radial pressure σ_r. VUMAT runs in conjunction with the ABAQUS and called every time the material properties are updated as the dynamic pressure field changes through time. Initial material properties (due to existing stress field because of winding) can be easily calculated via a wound-roll model. We employed the refinement explained above to the pressure data obtained from a 1D model like Hakiel's [4]. Thus, from 1D wound-roll model, we have harvested the initial radial pressure (E_r) data such that every element assigned the corresponding value with respect to its location along radial coordinate.

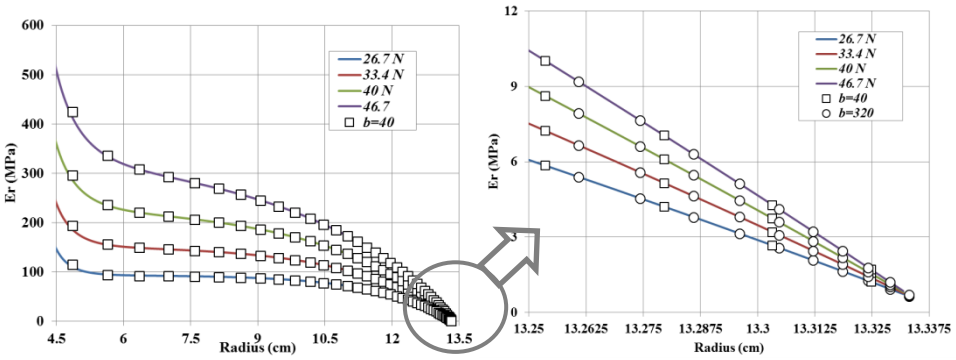

Figure 5 – PET1 Initial Radial Modulus E_r Sampling

Figure 5 shows sampling of initial radial modulus E_r for PET1 which is wound with different tensions. Values corresponding bias ratios *b=40* and *b=320* are shown under zoom. We have run the model for these two different materials under various refinements. Load-displacement-velocity-acceleration time curves are obtained for the rigid striker head. Corresponding Rho values were easily calculated by dividing the max deceleration values to 3.76g's.

In Figure 6 Impact force-time curves are given for different tensions both for PET1 and Pet2. We observe that total impact time is on the order of milliseconds. As K_2 and winding tension gets higher these curves becoming sharper. Fig 7. Shows the area under load-time curves that is impulse. In the device manual this value for a typical impact is given as 0.267 Ns.

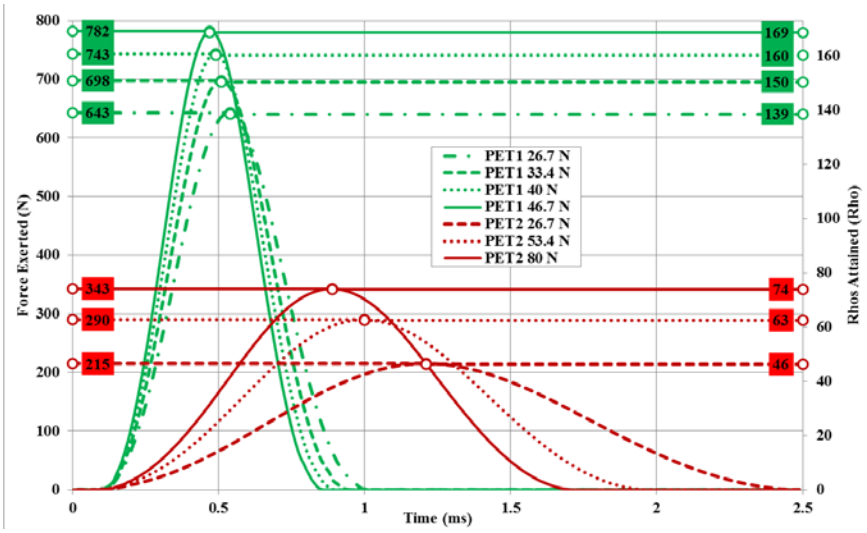

Figure 6 – ABAQUS Impact Force-Time Curves

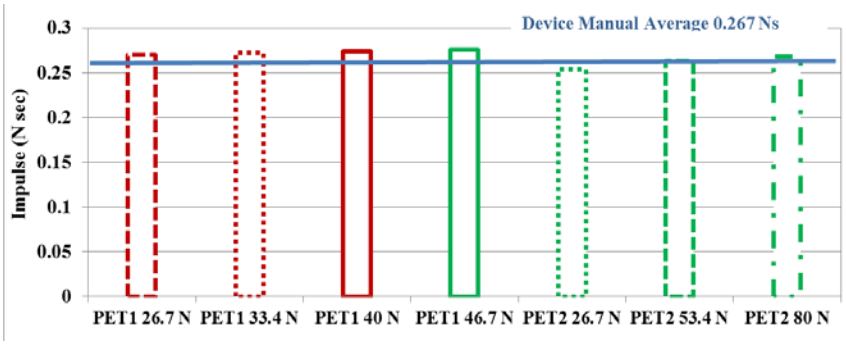

Figure 7 – 3D Impulse Values Obtained by Calculating the Areas under Load-Time Curves (Figure 6)

We see from Figure 7 that ABAQUS impulse values are very close to the value specified in the manual. This is a remarkable feature captured by the model because using different tension levels for two very different materials yielded very close values which are very close to device specified value on average. In Figure 8 effect of refinement and material nonlinearity are shown along with some test results for PET1.

It is evident from Figure 8 material nonlinearity during a dynamic pressure effect is crucial as no-update Rho values are significantly lower than the test results. Again from Figure 8 as the bias ratio increases it appears that finite element solutions converges. In fact with 40 radial sectors and bias ratio $b=320$ final model layers almost attain real layer thickness of 0.01 cm. Finally as roll becomes tighter it seems that test and model values approach. Figure 9 shows the same results for PET2. Here we observe significant deviations between model results and test results. When compared with PET1 results (Figure 8) it is apparent that harder materials yield more accurate results with the model. This may be explained by dynamic slippage around contact region as tremendous levels of stresses are developing and In ABAQUS we treated the roll as a continuous medium

without taking into account its actual layer-wise structure. Thus in reality occurrence of shear slippage is possible between layers very close to contact. We will address this issue in the discussion section.

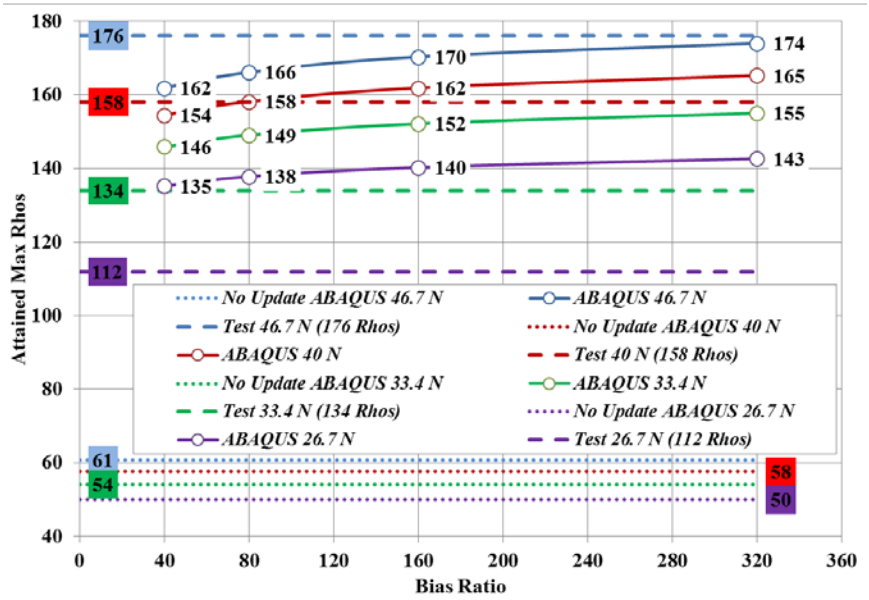

Figure 8 – PET1 Effect of Material Nonlinearity and Refinement on ABAQUS Results

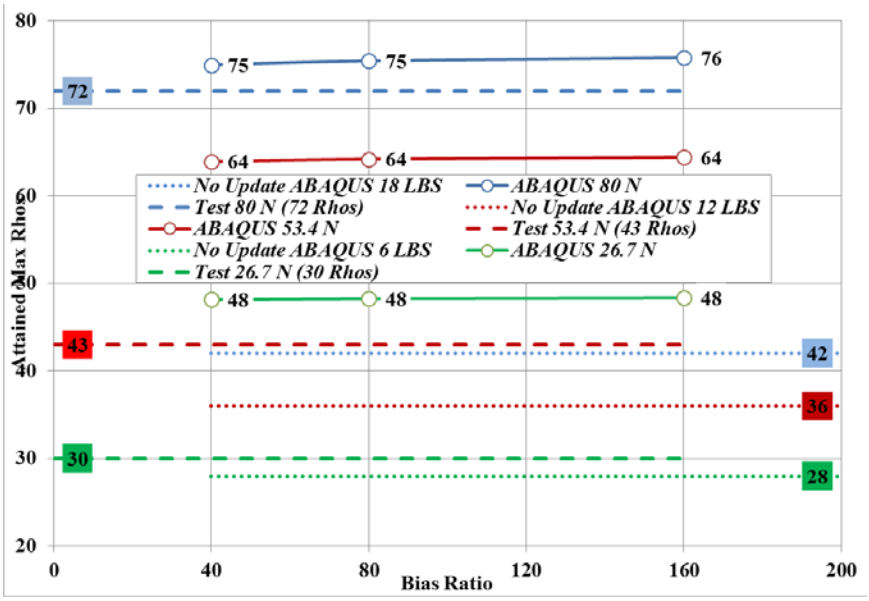

Figure 9 – PET2 Effect of Material Nonlinearity and Refinement on ABAQUS Results

In Figure 10 average dynamic pressures calculated beneath the impact location with different winding tensions are shown at the instant of max deceleration. It is observed that higher K_2 value results in harder rolls. Here it is also seen that tremendous pressure levels are attained during the impact event. The pressures are rapidly diminishing through inner sections of the roll and this is a clear manifestation of locality of the hardness measurements.

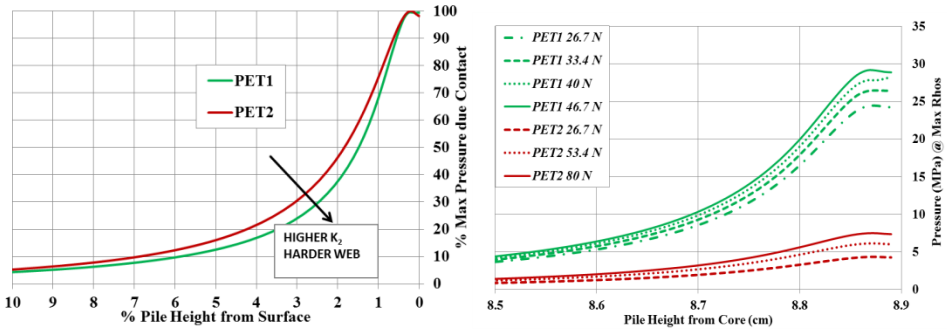

Figure 10 – Dynamic Pressures at the Instant of Max Deceleration

A 1.5D Model Based on Finite Differences

A simple 1D model of mass spring analogy can be used to represent striker and the roll side. We have already obtained striker spring stiffness and effective mass. Since pressure dependent, roll's spring stiffness should be nonlinear. The relation between load and displacement of a rigid nip pressed onto a roll, i.e. nonlinear spring character, can be obtained via curve fitting a second order polynomial to the load-deformation data generated by the algorithm which was developed in one of our previous studies [9]. The algorithm is based on 2D model which solves the nonlinear stress problem by considering a plane strain approach to the roll and the rigid object pressing onto it. Since we are using a 1D and 2D model in order to develop this simple hardness model we will call it a 1.5D model.

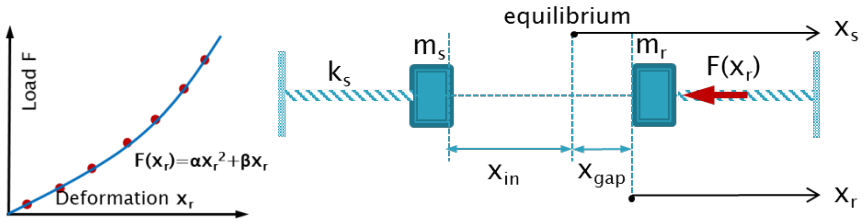

Figure 11 – 1.5D Hardness Model with Nonlinear Spring Stiffness

In Figure 11 k_s, m_s, k_r, m_r are stiffness and effective mass terms for spring and roll side respectively. x_{in} and x_{gap} are release and impact distances respectively from Table 1. x_s and x_r are spring and roll coordinates throughout motion. $F(x_r)$ is the nonlinear spring force representing the stiffness of the roll side:

$$F(x_r) = \alpha x_r^2 + \beta x_r \qquad \{3\}$$

Coefficients α and β are material and geometry specific parameters which are obtained by the contact algorithm developed in [9]. Because of geometrical discontinuity (gap distance) equation of motion should be written for two distinct regimes. That is before {4} (motion of striker alone) and after {5} impact (motion of both bodies together):

$$x_s \leq x_{gap} \rightarrow m_s\ddot{x_s} + k_s x_s = 0 \quad \{4\}$$

$$x_s > x_{gap} \rightarrow m_s\ddot{x_s} + k_s x_s + f = 0 \; and \; m_r\ddot{x_r} + F(x_r) - f = 0 \quad \{5\}$$

Here f is the contact force between striker and roll during bounded motion. Now because of geometrical compatibility between coordinates of striker and roll we can write down {6}:

$$x_r = x_s - x_{gap} \rightarrow \ddot{x_s} = \ddot{x_r} \quad \{6\}$$

Using {6}, {5} can be written in terms of x_s only:

$$(m_r + m_s)\ddot{x_s} + k_s x_s = -F(x_s - x_{gap}) \quad \{7\}$$

This simple equation of motion can be easily solved via finite differences. Defining time interval as $\Delta t = T/N$ where T is the total time and N is the number of total time steps. Generally $T=0.02$ s is enough for most cases i.e. max Rho is attained in this time. Now a central difference scheme for {4} and {7} can be written for $i=0,1,2,..,N$:

$$x_s \leq x_{gap} \rightarrow x_s^{i+1} = (2 - \frac{\Delta t^2 \, k_s}{m_s}) x_s^i - x_s^{i-1} \quad \{8\}$$

$$x_s > x_{gap} \rightarrow x_s^{i+1} = \left(2 - \frac{\Delta t^2 \, k_s}{m_s + m_r}\right) x_s^i - x_s^{i-1} - \frac{\Delta t^2}{m_s + m_r} F(x_s^i - x_{gap}) \quad \{9\}$$

Initial conditions can be specified as initial displacement being equal to release position and initial velocity being equal to zero:

$$x_s{}^0 = -x_{in} \quad \{10\}$$

$$v_s{}^0 = 0 \quad \{11\}$$

$$a_s{}^0 = -k_s \, x_{in}/m_s \quad \{12\}$$

In order to start {8} and {9} recurrence relations we need $x_s{}^{-1}$. Using {11} and {12} this can be approximated as:

$$x_s{}^{-1} = x_s{}^0 - \Delta t v_s{}^0 - \Delta t^2 a_s{}^0/2 \quad \{13\}$$

Central difference approximation is conditionally stable when $\Delta t < \sqrt{2m_s/k_s} \approx 0.01 \; s$. But since there is nonlinearity here $\Delta t = 0.00001 \; s$ is used. Now only thing left is the effective mass (m_r) for the roll. That is the portion of the roll's mass which is dynamically active during the impact. Here it is approximated via tapered pressure column approach. If we take a as the semi-contact width (calculated in 2D contact algorithm [9]) then pressure variation along a body due to Hertzian approach is [5]:

$$p(z) = p_{max}\frac{a}{\sqrt{a^2+z^2}} \quad \{14\}$$

Then at a depth z total force can be approximated as

$$p(z)A(z) \approx P \quad \{15\}$$

where P is the applied force per unit thickness at the surface and $A(z)$ is the effective area at depth z. From equilibrium it can be concluded that:

$$A(z) \approx 2\sqrt{a^2+z^2} \cong 2(z+a) \quad \{16\}$$

This gives a trapezoidal expansion trough depth z. Thus for depth $z=H$ (pile height) total unit thickness dynamically active roll volume V can be approximated as:

$$V = (2a+H)H \quad \{17\}$$

Now effective mass m_r can be calculated from the formula of the effective mass factor κ for tapered columns:

$$m_r = \kappa\rho_r V \quad \{18\}$$

where

$$\lambda = \frac{a}{a+H}\ ,\ \kappa = \frac{2\lambda^2(ln\lambda-1)ln\lambda+\lambda^2-1}{2(\lambda^2-1)(ln\lambda)^2}$$

Finally ρ_r is the mass density of the roll material. It is observed that results are rather insensitive to semi-contact width a and $0.6\ cm$ can accepted for hardness model.

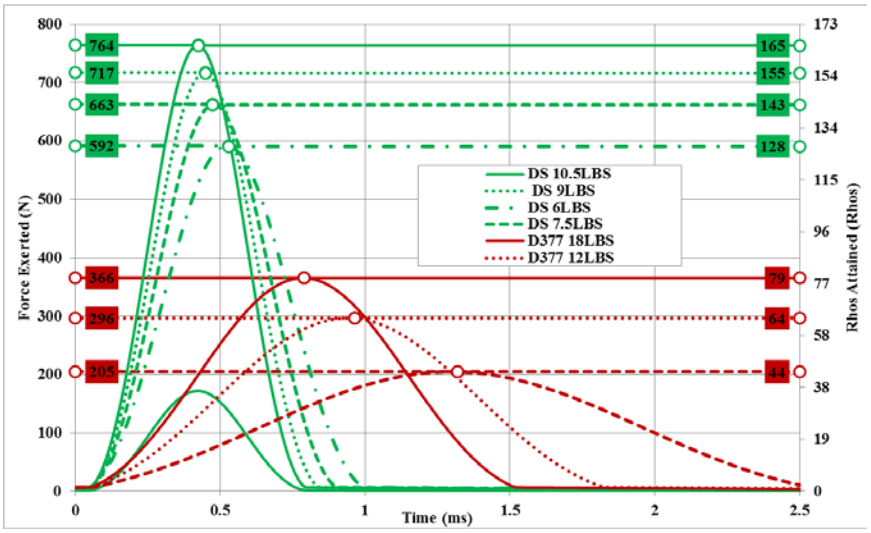

Figure 12 – Impact Force-Time Curves for 1.5D Model Based on Finite Difference Solution

Figure 12 shows force time curves calculated via finite difference solution. We observe that very close results are obtained when compared to sophisticated and demanding ABAQUS results (Figure 6).

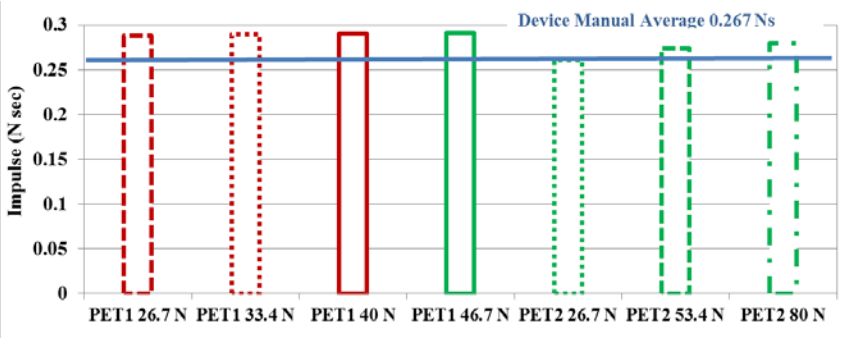

Figure 13 – 1.5D Impulse Values Obtained by Calculating the Areas under Load-Time Curves (Figure12)

1.5D Model-Energy Approach

Instead of solving equation of motion via finite differences we can use conservation of energy as well. Assuming the system is elastic during impact then conservation of energy requires:

striker_spring_elastic_energy@initial_position=

striker_spring_elastic_energy@max_depth + roll_elastic_energy@max_depth

Selected positions are zero velocity positions so there are only elastic potentials. If we define max depth the striker head attains (that is also the position for max Rhos) as δ_{max} then we can write down the energy equation as:

$$\frac{1}{2}k_s{x_{in}}^2 = \frac{1}{2}k_s(x_{gap}+\delta_{max})^2 + E_{roll}(\delta_{max}) \qquad \{19\}$$

where $E_{roll}(\delta)$ is the elastic energy stored in the roll spring. Since roll spring is nonlinear this can be calculated with the integration of the force deformation relation {3}:

$$E_{roll}(\delta) = \int_0^{\delta} F(\delta)d\delta \rightarrow E_{roll}(\delta_{max}) = \frac{\alpha{\delta_{max}}^3}{3} + \frac{\beta{\delta_{max}}^2}{2} \qquad \{20\}$$

Substituting {20} into {19} we will obtain a third order polynomial equation of δ_{max}:

$${\delta_{max}}^3 + \frac{3(\beta+k_s)}{2\alpha}{\delta_{max}}^2 + \frac{3k_s x_{gap}}{\alpha}\delta_{max} + \frac{3k_s}{2\alpha}\left(x_{gap}^2 - x_{in}^2\right) = 0 \qquad \{21\}$$

Here again we used the 2D contact algorithm developed in [9] and the geometry of this model retains on 1D spring mass representation. Thus we again called this one a 1.5D model. Now nonlinear equation {21} can be easily solved with one of the root finding methods like Newton-Raphson once α and β are known from the contact algorithm [9]. After the solution, newly found δ_{max} can be immediately used for calculating Rho_{max} i.e. Rho value for the maximum deceleration which in turn can be calculated from the maximum spring force $F(\delta_{max})$:

$$Rho_{max} = \frac{F(\delta_{max})}{(3.76\ g\ m_s)} \quad \{22\}$$

Here 3.76 appeared as 3.76 g = 1 Rho.

A GENERAL COMPARISON FOR MODELS', TEST RESULTS and LIMITATIONS

We have conducted Rho-meter tests on the wound rolls. Figure 14 shows results from models and tests together. The model 1.5D Energy is based on the conservation of energy were as model 1.5D is based on the finite differences solution. It seems models agree each other quite well. Taking the simplicity of 1.5D model, and its energy version which is even simpler, performance is quite remarkably when compared to highly demanding and sophisticated ABAQUS. In fact their success is based on the contact algorithm in [9]. It is also observed that as the roll becomes harder prediction accuracy improves

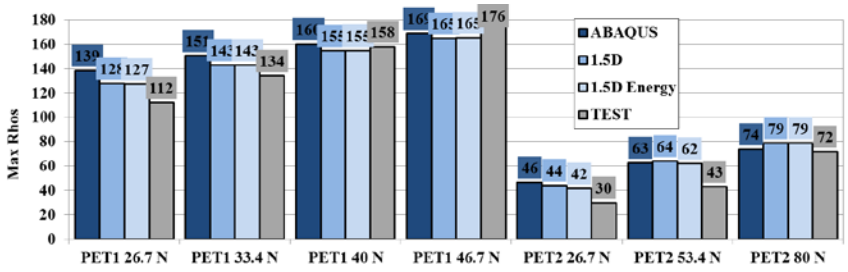

Figure 14 – Max Rho Values Compared from 1.5D Models, 3D ABAQUS Model and Tests

In Figure 15 Impulse values calculated with 1.5D finite difference model are shown with ABAQUS impulse values. They are in good agreement with the value of 0.267 Ns which is given in device manual as an average value for the impulse generated during impact of the striker.

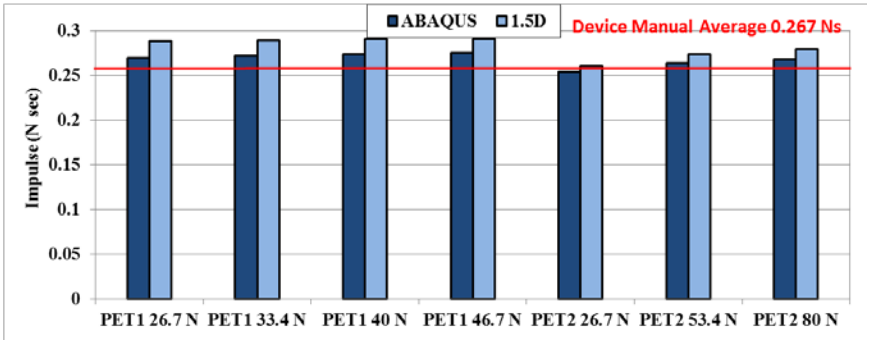

Figure 15 – Impulse values Compared from 1.5D Model and 3D ABAQUS Model

Another result which will be shown here is related with the effect of pile height. Figure 16 shows the pressure distributions of PET2 rolls wound with 53.4 N tension up to different pile heights.

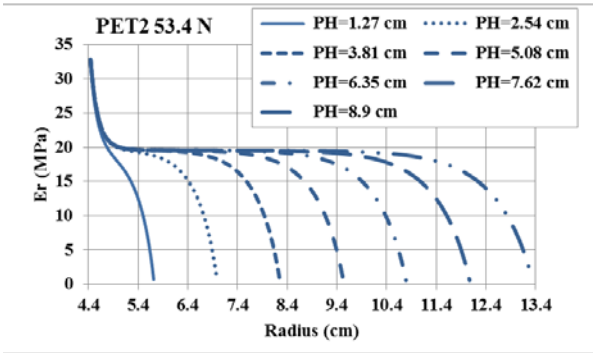

Figure 16 – Pressure Distributions inside PET2 Rolls with Different Pile Heights

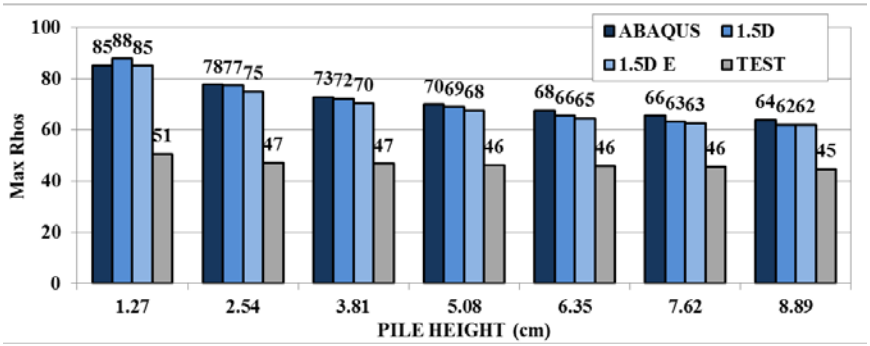

Figure 17 – Max Rho Values Calculated with Models and Test Results for PET2 rolls

We see that the results are very close to each other for various pile heights and this is also another proof that Rho-meter assessments of roll hardness are limited to the outer section of the roll. It is evident from Figure 14 and Figure 17 values from simulations and tests differs systematically for the "soft" PET2. As roll gets harder values come closer to the test results. Interlayer slippage is one of the possible explanations. The models assume roll body as a continuum without any layer-wise structure. Theoretically it is possible to model every layer individually with friction interface between them but this not possible in practice as the computational restrictions. Thus in order to show the effect of slippage we would consider a simple slip factor *SF* based on Coulomb friction model which indicates whether slip should be expected or not:

$$SF = \left| \frac{\sqrt{\tau_{rz}^2 + \tau_{r\theta}^2}}{\mu \sigma_r} \right| \qquad \{23\}$$

where μ is the dynamic coefficient of friction between layers, τ_{rz}, $\tau_{r\theta}$ are shear stresses along axial and tangential directions respectively. Now for regions where SF $\geq$ 1 slip is expected.

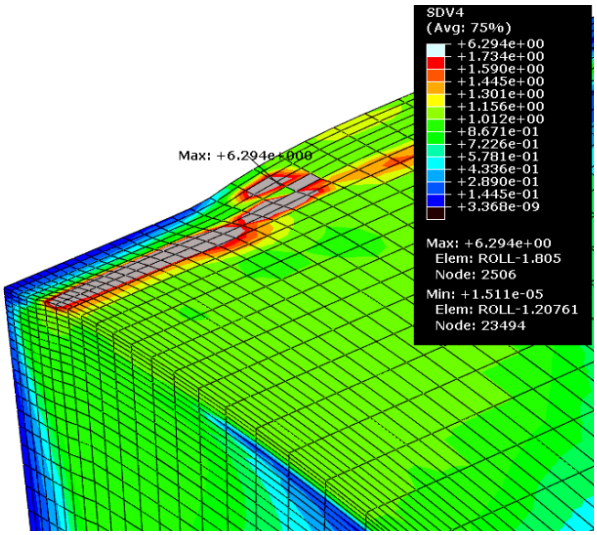

Figure 18 – Slip Factor Results for PET2 53.4 N

Figure 18 shows slip factor results for Pet2 wound at 53.4 N web line tension. For this we set coefficient of friction to a typical value $\mu=0.3$. It is evident that calculated shear factors are far greater than the shear carrying capacity i.e. SF>1 around impact zone. Thus for low K_2 materials like PET2 interlayer shear slippage effect seems to be an essential feature of the impact mechanics. Although we modeled the roll as a continuous body and used simple Coulomb friction model, slip factor levels shown indicates slippage and this might play a role in the systematic difference between model results and tests for Pet2. Nevertheless we can still introduce a simple approach for modeling the slippage without changing the roll bulk into a layer-wise structure. During the solution if we set the shear moduli G_{rz}, $G_{r\theta}$ to a very small value at the location where SF>1 is encountered than elements shear stiffness (shear carrying capacity) is diminished. Introducing a fictitious slippage by means of reducing shear stiffness we are able to emulate the interlayer "slippage" in the bulk of roll.

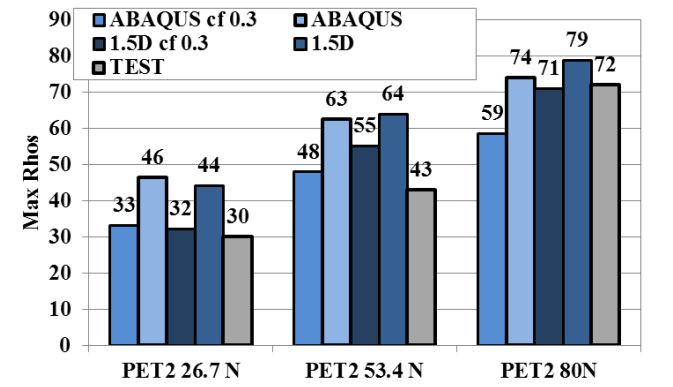

Figure 19 – Reduced Shear Stiffness Results for PET2

Figure 19 shows this simple approach of introducing shear slippage. As we see values come closer in this case. Nonetheless in the dynamic slippage, state and rate dependent types of friction may come into play. In fact coefficient of friction for the model is most likely different from the real one (coefficient of friction between actual layers) which is used for the interface slippage calculations as this value is more of a bulk property for roll continuum. Other possible explanations for the variation can be attributed to the wound roll material properties: Pfeiffer's constants (K_1 and K_2) are fitted to the stack pressure data generally much lower than the dynamic pressures roll experiences under striker. Thus at high pressures the Pfeiffer's constants might not represent the behavior correctly. In this aspect different material models can be tried which are proven to represent the correct physical behavior for high pressures. Another issue is the in-roll stresses towards the surface. Since Rho-meter tests hardness at this outer structure it is very important to get correct pressure distribution at the beginning for the initial radial modulus. Testing is required to validate the pressure variation of the outer roll structure so that we can be sure about the quality/fidelity of initial input for the impact problem.

INTEGRATED WOUND ROLL MODEL with HARDNESS SIMULATION

The main aim of this study is to bring together the engineering understanding of the mechanical state of a wound roll with practicality of the hardness quality testing. As indicated in the introduction roots of hardness testing comes from hitting a roll along CMD with an instrument and try to figure out hard and soft locations. These would correspond stress concentrations and give idea about CMD non-uniformities; mainly thickness variation. In one of the previous studies importance of length-wise persistent thickness variations over the stress field was shown [6]. An axisymmetric wound roll model for center-winding case was developed and thickness variation was represented via quadrilateral elements along CMD. A finite element formulation based on the notion of relaxation radius is applied and the incoming web line tension is allocated with respect to variable roll profile. Thus effect of thickness variation can be effectively dealt [6]. At the end of the solution entire stress field resulting from the non-uniformities within axisymmetric roll body is obtained. Now just like the application of contact algorithm in [9] to a plane strain roll model, each line of quadrilateral elements along radial direction can be taken as a sector i.e. plane strain roll. In this manner algorithm in [9] can be applied for each sector and we can effectively find α and β and nonlinear spring constants along CMD locations for each sector. Using 1.5D model based on energy conservation a Rho value can be obtained for each sector with expression {22}. That is just like the stress variation along CMD a Rho variation given for discrete points on CMD is produced.

K_1(Kpa)	K_2	E_z, E_θ (MPa)	web v_{zr}, $v_{\theta r}$	web $v_{z\theta}$	avg. Thick. (μm)	width (cm)
0	246.5	4999	0.01	0.3	76	61

roll inner rad. (cm)	roll out. Rad. (cm)	core inner rad. (cm)	E_{core} (Gpa)	core v_{zr}, $v_{\theta r}$, $v_{z\theta}$	T_w (Mpa)	P_{nip} (Mpa)
10.16	20.32	9.5	69	0.33	2.3 & 3.45	2.3

Table 3 – Material and Geometrical Data for CMD Thickness Variation Case

In order to demonstrate the integration of 1.5D hardness model into the axisymmetric wound-roll model we have used another PET material which has the properties in Table 3. Entire thickness profile of this web is mapped and used to produce rolls with tensions indicated in Table 3. Full thickness map and MD average thickness variation is given in Figure 20.

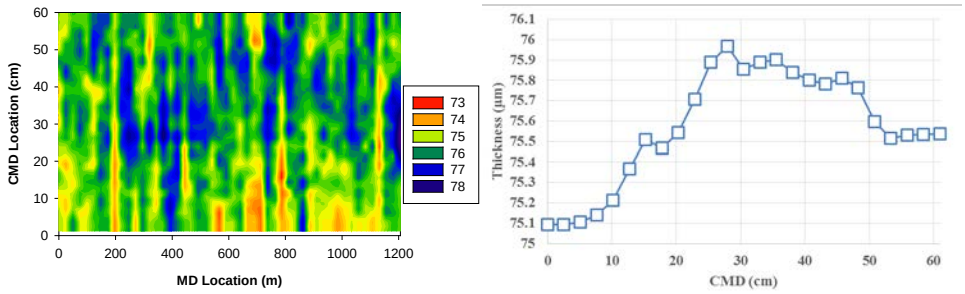

Figure 20 – Full Thickness Map and MD average Thickness Variation for Non-uniform PET

The pet film was intentionally produced with highly irregular thickness profile in order to study thickness variations. So this would be a good case for testing the ability of predicting “hard” and “soft” locations quantitatively on a roll. Figure 21 shows Rho results from tests and the integrated model. We see that integrated model is capable of capturing hardness variations along CMD and predicted levels agree well with the tests within reasonable limits. It is also remarkable how the Rho variation follows the same trend with MD average thickness variation of Figure 20. As basis for a future research topic we have advanced this formulation by the addition of nip effect. Thus for nip case tension allocation is based on the level of nip induced pressure at a CMD location. As we leave details in a planned dedicated study briefly during winding we can effectively find nonlinear spring counterparts for all sectors using contact algorithm [9]. In this manner nip impinged center-winding problem can be reduced to a beam (nip) on a nonlinear non-uniform elastic foundation (roll). As nip load is applied CMD nip pressure distribution can be used to allocate web line tension accordingly. Figure 22 shows results for nip impinged center-winding case. We see that model effectively captures the trend and level of Rho values.

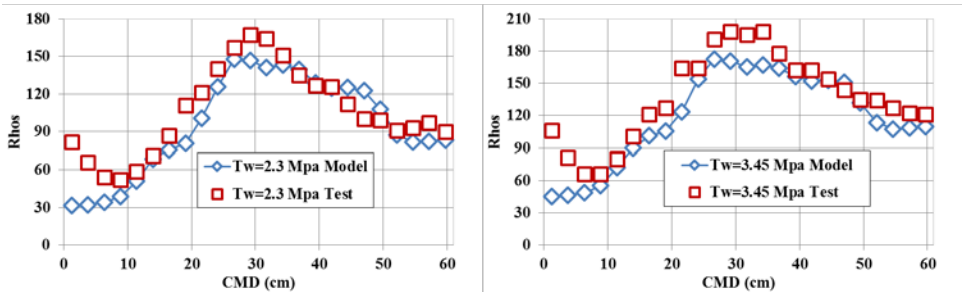

Figure 21 – Integrated Model and Rho-meter Test Results Center-winding w/o Nip

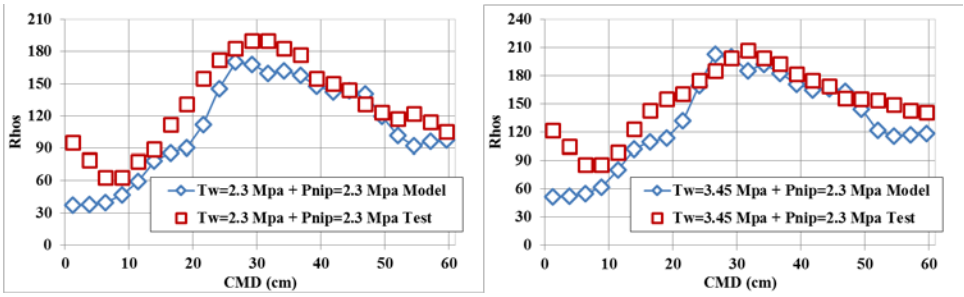

Figure 22 – Integrated Model and Rho-meter Test Results Center-winding w/ Nip

Integrated model contributes much to the assessment of the mechanical state of a wound roll. With the examples given it is proven that immediate realistic results can be produced in terms of quality measures with the simulations. Moreover as wound roll model produces stress and strain type engineering units and most of the defects are associated with excessive values of these engineering units, a direct quantitative relation between defects and hardness values has been established. Thus usefulness of hardness testing has been enhanced.

CONCLUSIONS

In this study we have methodically showed that modeling of Rho-meter is physically sound by independently modeling the striker side and the roll side. We have developed a ABAQUS VUMAT file for wound roll state dependency modeling during impact. This VUMAT can also be used for other web handling research applications. Also material models other than Pfeiffer's can also be included easily. We have run extensive parametric studies in order to simulate Rho-meter tests which were conducted on two different pet materials one with high the other with low K_2's. We have developed a 1.5D impact model which incorporates the contact algorithm [9] as the calculator of roll nonlinear stiffness which was crucial in its success. Two versions of 1.5D model (equation of motion based finite difference and energy based versions) are developed. Both versions performed remarkably with respect to sophisticated and demanding ABAQUS. For Rho tests we have obtained reasonably well prediction for high K_2 material. Investigation of the variation between model and test results for low K_2 material revealed interlayer slippage is becoming important by utilizing Coulomb type friction model. A simple shear stiffness limitation in order to emulate suspected interlayer

slippage is also proposed. As an important contribution we quantitatively showed that Rho-meters is measuring local hardness at the outer surface of the roll. Finally we integrated the hardness model with an axisymmetric wound roll model and thus turned qualitative hardness testing into quantitative by establishing the link between Rho's and stresses.

REFERENCES

1. Good, J. K., and Roisum, D. R., Winding: Machines, Mechanics and Measurements, DEStech Publications, Inc., Lancaster, Pennsylvania, 2008.
2. Pfeiffer, J. D., "Hardness Tester," United States Patent Office, February, 1969, 3,425,267.
3. Richard, J. A., Scott, A. B., David, D. R., and William, K. O., Method and Apparatus for Quantitatively Evaluating Roll Hardness, United States Patent Office, January 1992, 5,079,728.
4. Hakiel, Z., "Nonlinear Model for Wound Roll Stresses," Tappi, Vol. 70, No. 5, 1987, pp. 113-117.
5. Timoshenko, S., Theory of Elasticity, 3rd Ed., McGraw-Hill Pub, 1970.
6. Mollamahmutoglu, C., and Good J. K., "Modeling the Influence of Web Thickness and Length Imperfections Resulting from Manufacturing Processes on Wound Roll Stresses," Journal of Manufacturing Science and Technology, Vol. 8, Jan. 2015, pp. 22-33.
7. Good, J. K., "Modeling Rubber Covered Nip Rollers In Web Lines," Proceedings of the Sixth International Conference on Web Handling, June 2001, Oklahoma State University, pp. 159-186.
8. Pfeiffer, J. D., "Internal Pressures in a Wound Roll of Paper," Tappi, Vol. 51, August 1966, pp. 176-179.
9. Mollamahmutoglu, C., Good J. K., "Surface Compression of Wound Rolls". Proceedings of the Twelfth International Conference on Web Handling, 2013, Oklahoma State University.